Deep underground measurement of math xmlns="http://www.w3.org/1998/Math/MathML">mmultiscripts>mi mathvariant="normal">B/mi> mprescripts>/mprescripts>none>/none>mn>11/mn>/mmultiscripts>mo>(/mo>mi>α/mi>mo>,/mo>mi>n/mi>mo>)/mo>mmultiscripts>mi mathvariant="normal">N/mi>mprescripts>/mprescripts>none>/none>mn>14/mn>/mmultiscripts>/math>

Tyler C. Borgwardt, Richard James deBoer, Axel Boeltzig, Manoel Couder, Joachim Görres, August Gula, Mark Hanhardt, Khachatur V. Manukyan, Thomas Kadlecek, Daniel Robertson, Frank Strieder, and Michael Wiescher

Phys. Rev. C **108**, 035809 — Published 25 September 2023

DOI: 10.1103/PhysRevC.108.035809

Deep underground measurement of ^{11}B$(\alpha, n)^{14}$N

Tyler C. Borgwardt,[1,*] Richard James deBoer,[2] Axel Boeltzig,[2,3] Manoel Couder,[2] Joachim Görres,[2] August Gula,[4] Mark Hanhardt,[1,5] Khachatur V. Manukyan,[2] Thomas Kadlecek,[1] Daniel Robertson,[2] Frank Strieder,[1] and Michael Wiescher[2]

[1] *Department of Physics, South Dakota School of Mines & Technology, Rapid City, SD 57701, USA*
[2] *Department of Physics and Astronomy and the Joint Institute for Nuclear Astrophysics, University of Notre Dame, Notre Dame, Indiana 46556, USA*
[3] *Helmholtz-Zentrum Dresden-Rossendorf (HZDR), 01328 Dresden, Germany*
[4] *ISR-1, ISR Division, Los Alamos National Laboratory, PO Box 1663, Los Alamos, NM 87545, USA*
[5] *South Dakota Science and Technology Authority, Sanford Underground Research Facility, Lead, SD, 57754, USA*

(Dated: August 30, 2023)

The primordial elemental abundance composition of the first stars leads to questions about their modes of energy production and nucleosynthesis. The formation of ^{12}C has been thought to occur primarily through the 3α process, however, alternative reaction chains may contribute significantly, such as ^{7}Li$(\alpha, \gamma)^{11}$B$(\alpha, n)^{14}$N. This reaction sequence cannot only bypass the mass $A = 8$ stability gap, but could also be a source of neutrons in the first star environment. However, the efficiency of this reaction chain depends on the possible enhancement of its low energy cross section by α-cluster resonances near the reaction threshold. A new study of the reaction ^{11}B$(\alpha, n)^{14}$N has been undertaken at the CASPAR underground facility at beam energies from 300-700 keV. A 4π neutron detector in combination with pulse shape discrimination at low background conditions, resulted in the ability to probe energies lower than previously measured. Resonance strengths were determined for both the resonance at a laboratory energy of 411 keV, which was measured for the second time, and for a new resonance at 337 keV that has been measured for the first time. This resonance, found to be significantly weaker than previous estimates, dominates the reaction rate at lower temperatures ($T < 0.2$ GK) and reduces the reaction rate in first star environments.

I. INTRODUCTION

The study of the ^{11}B(α,n)^{14}N reaction has been discussed in the past as an important reaction for nucleosynthesis [1] in the framework of inhomogeneous Big Bang models [2, 3], in which ^{11}B would have been produced by a sequence of neutron and α-capture reactions and would have become the seed of a Big Bang r-process pattern. However, a more detailed analysis of the nucleosynthesis in such a scenario [4] and the abundance patterns in early stars [5, 6] have demonstrated that this model is not sustainable [7].

Sparking renewed interest, it has been proposed recently that the ^{11}B$(\alpha, n)^{14}$N reaction may also play a role in helium burning environments in first generation stars [8]. The ^{11}B isotope represents an important node in a network of proton and α-induced reactions as well as electron capture processes that leads to its establishment as a stepping stone for subsequent α-induced reactions such as ^{11}B$(\alpha, p)^{14}$C or ^{11}B$(\alpha, n)^{14}$N feeding the CNO mass range. The strength of the break-out from standard helium burning depends not only on the nuclear reaction rates involved in the reaction pattern, but also on deep convection and the evolution of helium enriched bubbles in the early star environments [9]. It is a rather complex and dynamic nucleosynthesis environment. The deep convective mixing patterns, as well as the strength on the different reaction branches, play a critical role in the on-set of this environment and the resulting abundance distribution of early stars [5, 6].

The α-induced reactions are facilitated by resonance contributions of triton-alpha cluster configurations [10] in the ^{15}N compound nucleus, emerging in the excitation range near the α-threshold. The direct study of these states requires very low energy measurements of the various reaction branches and a reliable R-matrix analysis of the data over a wide energy range for many reaction channels [11, 12].

The α-induced reactions may also play an important role on the operation of boron-fusion reactors [13], which are based on the ^{11}B$(p, 2\alpha)^{4}$He reaction, converting boron fuel into three free α-particles with a kinetic energy distribution between 2 and 4 MeV corresponding to the 8.7 MeV difference in binding energy of the initial and final system [14, 15]. The free α-particles distribute their kinetic energy rapidly to the plasma by ^{11}B$(\alpha, \alpha')^{11}$B inelastic scattering but can also undergo α-induced nuclear reactions with the ^{11}B isotopes in the plasma environment. To understand the role and potential impact of these secondary reactions and the consequences for the build-up of impurities in the specific reactor environment, these processes need to be investigated over a wide energy range.

In both the case of a convective stellar plasma environments in first stars and boron fusion reactor operation, the ^{11}B$(\alpha, n)^{14}$N reaction is of particular interest as a

* tyborg@lanl.gov; Present address: NEN-2, NEN Division, Los Alamos National Laboratory, Los Alamos, NM 87545, USA

neutron source, resulting in a new neutron capture reaction pattern leading to the production of short-lived nuclei from the existing seed material, rapidly creating heavier elements.

In this paper we present new results on α-capture on ^{11}B by probing the ^{11}B$(\alpha,n)^{14}$N reaction at very low energies, complementing our previous study of the reaction at higher energies [16]. An earlier study by Wang *et al.* [1] was handicapped by cosmogenic neutron background and, therefore, did not reach the desired low energy range. To reduce the background of cosmic ray induced neutrons in our experiments, we have studied the reaction at the CASPAR facility [17], located 4850 ft deep underground at the Sanford Underground Research Facility (SURF).

In the following section we describe the experimental approach for studying the ^{11}B$(\alpha,n)^{14}$N reaction over the energy range (energies are in the lab frame unless otherwise noted) between 300 and 700 keV, followed by an analysis of the resonance features of the reaction in comparison to the resonance analysis of the ^{11}B$(\alpha,p)^{14}$C study by Gula *et al.* [18] in Sec. IV. To capture the effect of our newly measured strength for the $E_\alpha = 337$ keV resonance, which is significantly different from previous theory estimates, a revised reaction rate is presented in Sec. V. Concluding remarks are given in Sec. VI.

II. EXPERIMENTAL METHODS

The ^{11}B$(\alpha,n)^{14}$N reaction was investigated from $E_\alpha =$ 300-700 keV using the JN accelerator at the CASPAR underground laboratory [17]. Beam intensities of He$^+$ ions ranged between 60-70 µA. The beam energy was calibrated to better than 1 keV using resonances in the ^{27}Al(p,γ)^{28}Si reaction and was monitored using the narrow resonance at $E_\alpha = 606$ keV in the ^{11}B$(\alpha,n)^{14}$N reaction. Three thick boron targets were used. These targets were created by vacuum evaporation of 99 % enriched ^{11}B powder onto a 0.5 mm Ta backing. The target thicknesses were determined by performing thick-target resonance scans over the narrow resonance at $E_\alpha = 606$ keV. The targets were observed to have an energy loss between 60-90 keV at this energy. Target degradation was monitored by performing repeated scans of the $E_\alpha = 606$ keV resonance. After accumulating ≈ 2 C of integrated charge, no significant degradation was observed.

Yields from the ^{11}B$(\alpha,n)^{14}$N reaction were measured using a 4π neutron detector with a polyethylene moderator ($30.5 \times 30.5 \times 33\,\text{cm}^3$) and 5 % borated polyethylene shielding (5 cm). The detector has been described previously [19] and its current configuration was described in Borgwardt [20]. A background rate of 0.1 counts per second in the underground laboratory environment at CASPAR was observed. The polyethylene moderator houses two concentric rings of ^{3}He proportional counters, containing a total of 16 detectors. The polyethylene moderates neutrons to thermal energies, which are then detected through the electrical signal induced by the ^{3}He$(n,p)^3$H reaction. The efficiency of the detector was determined through previous measurements of the ^{51}V$(p,n)^{51}$Cr reaction [19], as well as modeling and a measurement of a ^{252}Cf source [20]. For the neutron energies relevant to this work (300-600 keV), the efficiency was found to be 31-34 %. For neutrons coming from high spin states, such as the lowest energy state measured in this work, the neutron detection efficiency needs to account for the highly anisotropic angular distribution. This was done through simulation and resulted in a reduction of the efficiency by 10 % (e.g., 34 % to 31 %) for the $E_\alpha = 337$ and 606 keV states.

Pulse shape discrimination was used to mitigate the intrinsic α-activity of the detectors using the rise time discrimination method [21, 22]. Further details of the implementation can be found in Borgwardt [20]. The pulse shape discrimination rejected 99 % of the intrinsic background of the detectors, while preserving 35 % of the neutron signal. The uncertainty in the efficiency, over the limited neutron energy range of the present experiment, is estimated to be 10%, largely due to the ^{51}V$(p,n)^{51}$Cr calibration that produces neutrons at a very similar energy.

III. DATA ANALYSIS

The resulting yields with and without pulse shape discrimination (PSD) are shown in Fig. 1 and an example of the PSD can be seen in Fig. 2. The stoichiometry of the targets was assumed to be pure boron, which had a stopping power of 50-60 $(\text{eV}\,\text{cm}^2)/10^{15}$ atoms over the energy range of the measurements. A 10% uncertainty is estimated, based on oxidation levels of targets used in previous studies [23, 24].

Resonance strengths were derived using two methods, first from the yield curves of the two low energy resonances using the isolated narrow resonance formalism and then through an R-matrix fit of the unfolded cross section data as discussed in more detail in Sec. IV. The two methods resulted in consistent values. The yield from the underlying background of the broad resonance at $E_\alpha = 596$ keV was calculated and subtracted off when deriving the resonance strengths. As a broad resonance, it was found that the width could not be treated as constant and had to be corrected for the penetrability. The resonance strength was found to be 1.3 times larger than that reported by Wang *et al.* [1].

Yield data were converted to cross sections following the methods in [25] and Brune and Sayre [26] using:

$$\sigma_{\text{exp}}(E_{\text{eff}}) = \frac{Y(E_0)}{f n_x}, \quad (1)$$

where n_x is the number of active target nuclei, Y is the yield at beam energy E_0, and E_{eff} is the effective energy and f is a correction factor, as defined in Brune and Sayre

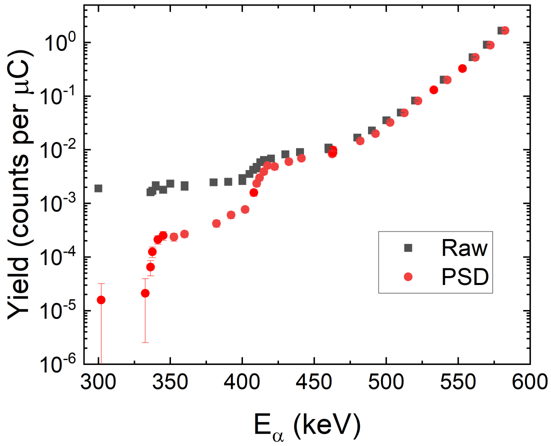

FIG. 1: Thick target yield curve. The raw data is shown in black, while the red points indicate the data after pulse shape discrimination has been applied. Two resonances can be seen in the data, which resemble step functions and are on top of the tail of the broad resonance at $E_\alpha = 596\,\text{keV}$. The front (low energy) edge of each step function can be used to determine the resonance energy, while the maximum yield at the plateau determines the resonance strength.

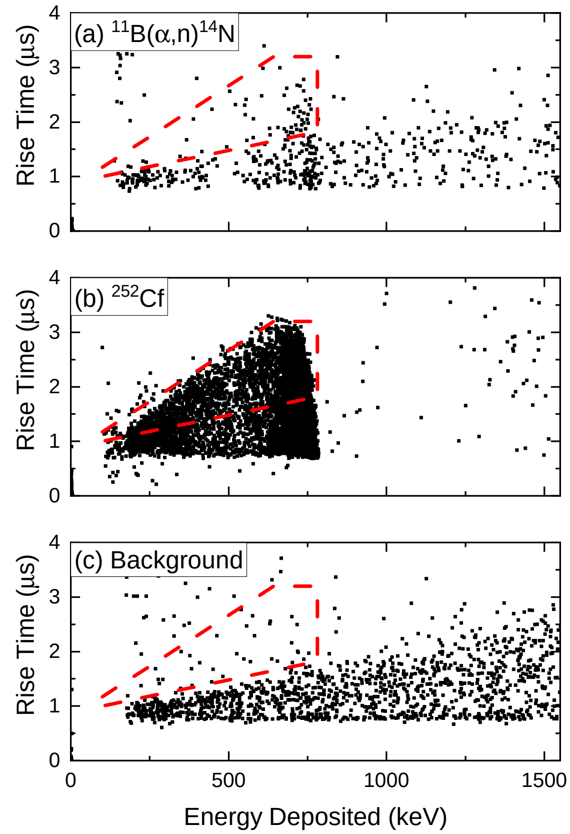

FIG. 2: Pulse shape discrimination of the (a) measured data at $E_\alpha = 350\,\text{keV}$. The total signal consisted of 1445 events in a 2.5 hour measurement. Inside the cut window is 60 events with an expected background of 15 events. Pulse shape discrimination of (b) a ^{252}Cf source and (c) laboratory background were used to define a cut window (red dashed line).

TABLE I: Summary of the primary sources of systematic uncertainty for the $^{11}\text{B}(\alpha,n)^{14}\text{N}$ cross section data of this work.

Systematic Uncertainty Contribution	%
Stopping Power	10
Efficiency	10
Resolution Unfolding	5
Beam Current	3
Total	15

[26]. The cross section data are shown in Fig. 3. The main systematic uncertainty contributions to the cross section are summarized in Table I.

IV. *R*-MATRIX FIT

The R-matrix description of the $^{11}\text{B}(\alpha,n)^{14}\text{N}$ cross section is a complicated case. The de-excitation of levels populated over the energy range of the present data can proceed through not only the α-particle and neutron channels, but also through the proton channel. Thus a multichannel analysis is required. In addition, many broad higher energy resonances exist that contribute to the slowly varying underlying cross section. In the analysis of Wang *et al.* [1], a more simplified multilevel Breit-Wigner analysis is used, but this does not include important interference contributions. To better model the cross section, a multichannel R-matrix analysis is employed in this work, building off of previous R-matrix descriptions of the ^{15}N system [27–30] that focused solely on $^{14}\text{N}+\text{n}$ reactions. The fit is limited to the low energy range covered by the $^{11}\text{B}(\alpha,n)^{14}\text{N}$ data of this work, but considers data from $^{14}\text{N}+\text{n}$, $^{11}\text{B}+\alpha$, and $^{14}\text{C}+\text{p}$ reactions available in the literature. This analysis uses the code `AZURE2` [31, 32] and is based on previous calculations given in deBoer *et al.* [16]. Observable resonance parameters are used directly by way of the alternative R-matrix parameterization of Brune [33]. Masses were taken from the 2020 AME mass evaluation [34, 35] and the channel radii in fm are 5.1, 4.3, and 4 for $(^{11}\text{B}+\alpha)$, $(^{14}\text{C}+\text{p})$, and $(^{14}\text{N}+\text{n})$, respectively.

To obtain an R-matrix description of the relevant energy region, a selection of data has been used that covers several different reaction channels. While there are several additional data sets available in the literature [1, 36–

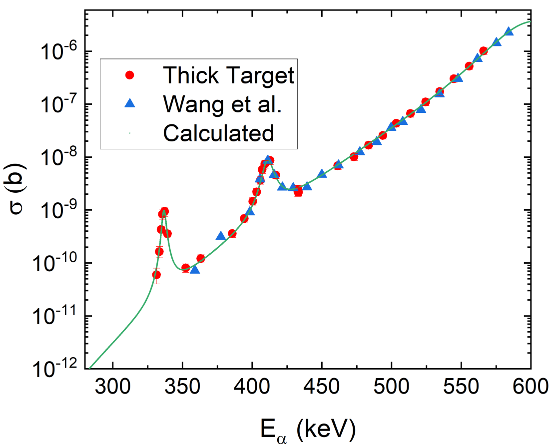

FIG. 3: Cross Section of the ^{11}B$(\alpha,n)^{14}$N reaction. The data of Wang *et al.* [1] have been scaled by a factor of 1.3 as described in the text.

46], a selected set of data is used in order to not overly complicate the present work. A more comprehensive re-evaluation of the ^{15}N compound system at low energies is underway [47], but is beyond the scope of this work.

The R-matrix analysis includes the representative data sets for ^{14}N+n total neutron cross section data of Harvey *et al.* [42], the ^{14}N$(n,p)^{14}$C data of Morgan [44], and proton scattering on ^{14}C data of Harris and Armstrong [36]. These data sets are used because they minimized distortions due to target energy loss effects, are relatively consistent with one another, and provided uncertainty information.

The fitted data sets are shown in Fig. 4 where the two lowest energy resonances in the ^{11}B$(\alpha,n)^{14}$N reaction are indicated. The data sets in the other reaction channels are compared on a common ^{15}N system excitation energy scale. Two resonances are clearly visible in the ^{11}B$(\alpha,n)^{14}$N data at E_α = 337 and 411 keV. The low energy tail of a broader, higher energy, resonance is also evident, which corresponds to the 596 keV resonance. Comparing to the ^{14}N$(n,p)^{14}$C, ^{14}C$(p,p)^{14}$C, and ^{14}N+n total cross section data (^{14}N(n,total)), corresponding resonances in these reactions are readily apparent.

The total neutron cross section data of Harvey *et al.* [42] was an important data set for the R-matrix fit because total neutron cross section measurements can typically be made with significantly higher accuracy and precision than other types of reaction studies. For the present analysis, the total neutron cross section data were limited to $E_n < 0.8$ MeV, which encompasses the excitation energy range of the ^{11}B$(\alpha,n)^{14}$N data of this work and also extends to somewhat lower energies. These data are crucial for the fit because the two lowest energy resonances observed in the ^{14}N(n,total) data correspond to the same levels ($E_\text{x} = 11.24$ MeV ($7/2^+$) and 11.29 MeV ($1/2^-$)) as the two lowest energy resonances observed here in the ^{11}B$(\alpha,n)^{14}$N data. Because of their small uncertainties, the ^{14}N(n,total) data precisely constrain the energy and width of the resonances. In addition, these data constrain the energy and width of the level at $E_\text{x} = 11.43$ MeV ($1/2^+$, $E_\alpha = 596$ keV), which is responsible, in large part, for the underlying "non-resonant" component of the observed ^{11}B$(\alpha,n)^{14}$N cross section. The ^{14}N(n,total) data also supplies a very stringent cross check of the energy calibration of the ^{11}B$(\alpha,n)^{14}$N data.

For the ^{14}N$(n,p)^{14}$C reaction, the data set of Morgan [48] was utilized because of its high energy resolution and detailed uncertainty information. The two clear resonances observed in this data set correspond to the levels at $E_\text{x} = 11.29$ MeV and 11.43 MeV. However, another even broader (E_α = 827 keV, $\Gamma \approx 320$ keV) underlying resonance is also present that is not clearly visible in the data but is needed to reproduce the shape of the cross section, which corresponds to a $1/2^+$ level at $E_\text{x} = 11.60$ MeV. This very broad resonance can be observed clearly in the higher energy proton scattering data of Harris and Armstrong [36] (not shown in Fig. 4). This very broad resonance also contributes to the underlying "non-resonant" portion of the ^{11}B$(\alpha,n)^{14}$N cross section. The cross sections are compared, on their common excitation energy scale, in Fig. 4. Table II contains the best fit parameters for the two lowest energy resonances.

From the widths deduced here, the spectroscopic factors for the α-cluster as well as the single particle components of the resonance levels can be extracted. They are shown in Table III. The results indicate that the level at $E_\text{x} = 11.24$ MeV, corresponding to the resonance at $E_\alpha = 336.7$ keV should have a $J^\pi = 7/2^+$ spin parity assignments to meet the Wigner-limit for the proton spectroscopic factor. Table III suggests the state has a pronounced α-cluster configuration and will be, together with the $J^\pi = 1/2^+$ level at $E_\text{x} = 11.43$ MeV, corresponding to the resonance at $E_\alpha = 596.5$ keV, a near threshold α-cluster state.

The low energy extrapolation of the S-factor for the ^{11}B$(\alpha,n)^{14}$N reaction is shown in Fig. 5. Below the two resonances at E_r = 337 and 411 keV, the slowly varying S-factor, as modeled by the R-matrix analysis, is determined by the low energy tails of broad, higher energy resonances. The experimental data of this work do not indicate any strong subthreshold state contributions, which is consistent with previous transfer studies that do not report any strong α-cluster states near the threshold [52, 53]. However, the ^{11}B$(^7$Li$,t)^{15}$N α-transfer measurements of both Kohler *et al.* [52] and Norton *et al.* [53] do indicate that the sub-threshold state at E_x = 10.7019(3) MeV [54] (E_α = -290 keV) has at least a moderate α-strength. To estimate the contribution that this state could have on the low energy S-factor, this state's α-particle Asymptotic Normalization Coefficient (ANC) was increased until its contribution to the S-factor resulted in an increased cross section similar to the 84% upper bound obtained from the `BRICK` [49] MCMC uncertainty analysis (ANC$_\alpha$ = 3000 fm$^{-1/2}$). This state

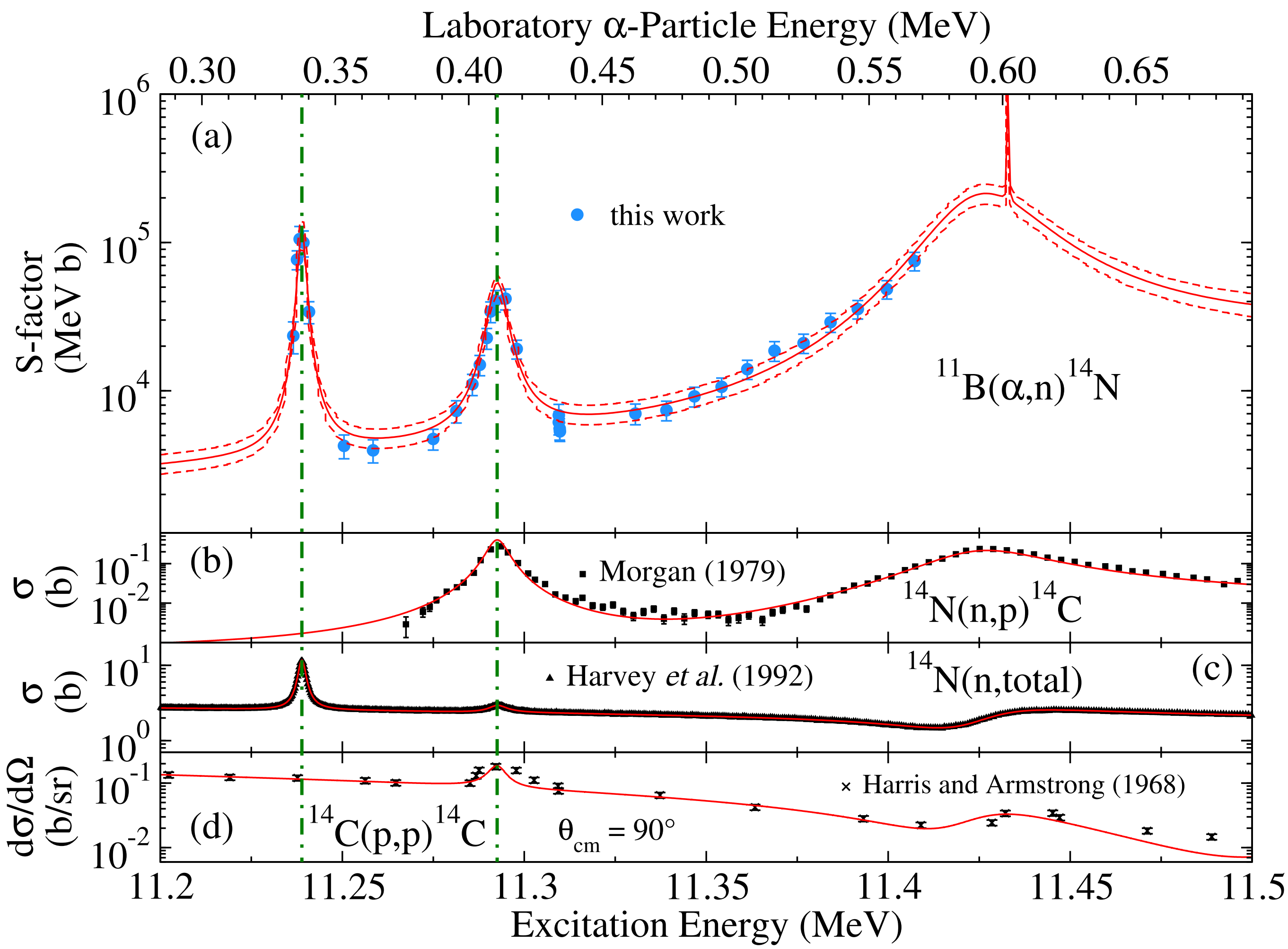

FIG. 4: Simultaneous `AZURE2` R-matrix fit (red solid lines) to reactions that populate the ^{15}N system near the α-particle separation energy for (a) the ^{11}B$(\alpha,n)^{14}$N data of this work, (b) the ^{14}N$(n,p)^{14}$C data of Morgan [48], (c) the ^{14}N(n,total) data of Harvey *et al.* [42], and (d) the ^{14}C$(p,p)^{14}$C data of Harris and Armstrong [36]. The green vertical dashed-dotted lines indicate the energies of the two states populated by the two lowest energy resonances in the ^{11}B$(\alpha,n)^{14}$N study described here. The dashed red lines in a) represent the 16 and 84% quantiles resulting from the `BRICK` [49] uncertainty analysis.

TABLE II: Resonance parameters obtained for the two lowest lying resonances in the ^{11}B$(\alpha,n)^{14}$N data from a simultaneous R-matrix fit to data from the reactions ^{11}B$(\alpha,n)^{14}$N (this work), ^{14}N$(n,p)^{14}$C [48], ^{14}N(n,total) [50] and ^{14}C$(p,p)^{14}$C [36] data from the literature (see Fig. 4). Resonance energies are in the laboratory frame and are given in units of keV, while all other values are given in the center-of-mass frame in units of eV. The uncertainty in the resonance energies is dominated by the accelerator energy calibration.

E_r (keV)	J$^\pi$	$\omega\gamma_{(\alpha,n)}$ (eV) this work	$\omega\gamma_{(\alpha,n)}$ (eV) lit. value	Γ (eV)	Γ_α (eV)	Γ_n (eV)	Γ_p (eV)
336.7(10)	$\frac{7}{2}^{(+)\text{a}}$	6.3(9)$\times10^{-7}$	5.85 $\times$ $10^{-5\text{b}}$	2.38(1) $\times10^{3}$	3.2(5)$\times10^{-7}$	2.38(1) $\times10^{3}$	9(2)$\times10^{-3\text{c}}$
411.0(10)	$\frac{1}{2}^{-}$	1.6(3)$\times10^{-5}$	1.6(2)$\times10^{-5\text{c}}$	6.09(9) $\times10^{3}$	1.2(2)$\times10^{-4}$	1.61(2) $\times10^{3}$	4.48(8) $\times10^{3}$

[a] From Harvey *et al.* [50].
[b] Estimate of Caughlan and Fowler [51].
[c] From Wang *et al.* [1].

TABLE III: Excitation energies (E_x), spin and parity (J^π) as well as orbital momenta associated with the α + ^{11}B (ℓ_α) and p + ^{14}C (ℓ_p) partitions. The spectroscopic factors C^2S were calculated from the ratio of the observed partial width and the Wigner limits for the transition, which were calculated in the framework of a simple Coulomb potential model.

E_r (keV)	E_x (MeV)	J$^\pi$	ℓ_α	C^2S_α	ℓ_p	C^2S_p
336.7	11.239	$\frac{7}{2}^+$	2	7.8×10^{-3}	4	–
411.0	11.315	$\frac{1}{2}^-$	1	5.1×10^{-3}	1	1.10×10^{-2}
596.5	11.429	$\frac{1}{2}^+$	2	8.35×10^{-1}	0	4.10×10^{-3}
606.0	11.436	$\frac{7}{2}^-$	3	7.04×10^{-3}	3	7.50×10^{-8}

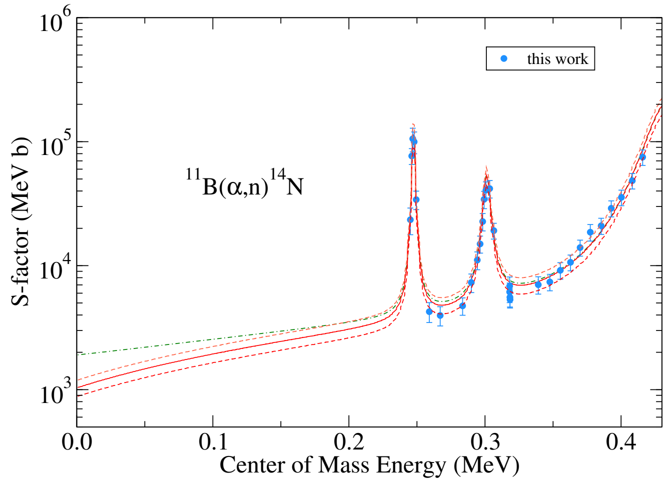

FIG. 5: Extrapolation of the low energy S-factor for the ^{11}B$(\alpha,n)^{14}$N reaction. The green dashed-dotted line represents a possible contribution from the subthreshold state at $E_x = 10.7$ MeV. Descriptions of the other components of the plot can be found in Fig. 4.

is only proton unbound ($S_p = 10.21$ MeV) and its proton width (Γ_p) was kept fixed at a value of 200 eV [54]. This state's neutron ANC$_n$ (0.07 fm$^{-1/2}$) was estimated by fitting the very low energy ^{14}N$(n,p)^{14}$C data of Koehler and O'Brien [55], as shown previously in deBoer *et al.* [16].

While the subthreshold state at $E_x = 10.7019(3)$ MeV seems to be the most likely candidate to produce an S-factor enhancement at low energy, the calculation shown in Fig. 5 is not unique as it is very possible that several subthreshold states sum to produce an enhancement of the low energy S-factor. However, after making test calculations for several other bound states, it was found that the energy dependence produced by all of them was similar. The energy dependence in each case was fairly smooth, indicating minimal interference effects. Given the phenomenological nature of the model used, interference effects can not be ruled out, but none were seen with the known levels in the energy region. Therefore, their summed contribution is fully constrained by the lowest-energy, off-resonance, cross section data of this work and a significantly larger low S-factor is not possible through this type of reaction mechanism. It is possible that an additional resonance could be present at very low energies, but its neutron width and α-particle reduced width would have to be small, given the constraints imposed by low energy ^{14}N(n,total) data and α-transfer data, respectively.

V. REACTION RATE

An updated reaction rate was calculated by numerical integration of the ^{11}B$(\alpha,n)^{14}$N R-matrix cross section and is shown compared to the rate of Caughlan and Fowler [51] in Fig. 6. The rate is available in tabulated form in the Supplemental Material [56]. The individual resonance contributions to the rate, in the absence of interference, are shown in Fig. 7. The newly observed resonance at 337 keV dominates the rate between approximately 0.1 and 0.2 GK. Because the strength of this resonance was estimated to be much larger by Caughlan and Fowler [51], the rate presented here is significantly lower over this temperature range. Below ≈0.1 GK, the rate is dominated by the low energy tails of higher lying broad resonances, which make up ≈50% of the total. As discussed in Sec. IV, subthreshold state contributions could also be present, which could also make a significant contribution to the low temperature rate as indicated in Fig. 7. At temperatures above ≈ 0.2 GK, the strong, narrow, resonance at $E_r = 606$ keV, which corresponds to the $7/2^-$ level at $E_x = 11.436$ MeV, dominates the reaction rate.

The ^{11}B$(\alpha,n)^{14}$N reaction dominates by at least an order of magnitude over the competing ^{11}B$(\alpha,p)^{14}$C reaction as indicated in Fig. 8. This suggests that the ^{11}B$(\alpha,n)^{14}$N reaction may contribute to neutron production in an early star environment facilitating the production of heavier isotopes by neutron induced reactions. However the overall neutron flux will be small because of the abundance of ^{11}B expected for the framework of nuclear reactions in an early star environment. The equilibrium abundance of ^{11}B will be established by the reaction rate ratio of the main ^{7}Li$(\alpha,\gamma)^{11}$B production reaction, the ^{11}B$(\alpha,n)^{14}$N depletion reaction towards the CNO range as presented here, and the dominant depletion process ^{11}B$(p,2\alpha)^4$He [57], which processes material

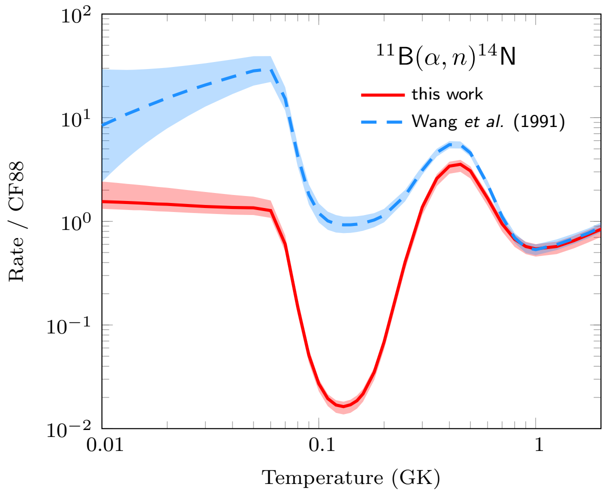

FIG. 6: Ratios of the rate of this work (solid red line) and that of Wang *et al.* [1] (blue dashed line) to that of Caughlan and Fowler [51] (CF88). The significant decrease in the rate at ≈0.1 GK from this work comes from the much smaller measured strength for the 337 keV resonance than that estimated by Caughlan and Fowler [51].

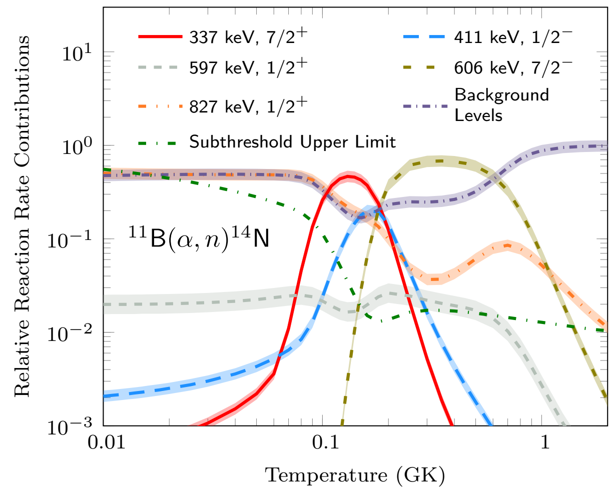

FIG. 7: Individual resonance components of the ^{11}B$(\alpha,n)^{14}$N reaction rate relative to the total. The upper limit of the subthreshold state contribution is also indicated.

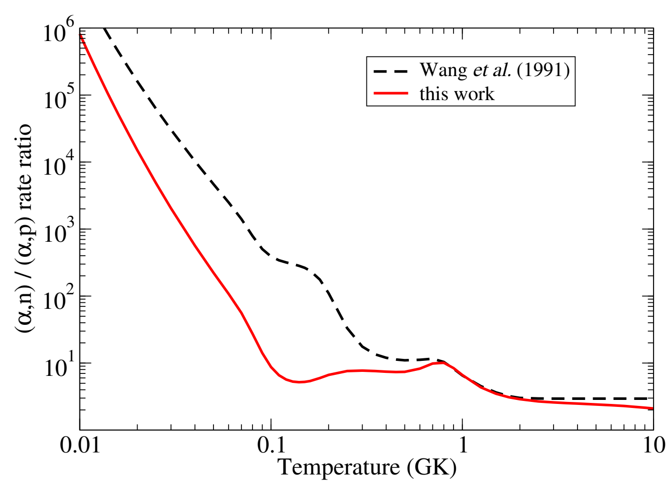

FIG. 8: Ratio of the ^{11}B$(\alpha,n)^{14}$N reaction rate of this work (red solid line) and from Wang *et al.* [1] (black dashed line) to the ^{11}B$(\alpha,p)^{14}$C reaction rate of Wang *et al.* [1].

back into helium feeding the production cycle again. The equilibrium abundance

$$\frac{[^{11}B]}{[^{7}Li]} \approx \frac{[^{4}He]\langle\sigma v\rangle_{^{7}Li(\alpha,\gamma)}}{[^{4}He]\langle\sigma v\rangle_{^{11}B(\alpha,n)} + [^{1}H]\langle\sigma v\rangle_{^{11}B(p,3\alpha)}} \qquad (2)$$

is likely low, as shown in Fig. 9, because of the relatively strong ^{11}B$(p,3\alpha)$ depletion reaction. However, this ratio also depends on the abundances of ^{7}Li as well as ^{4}He and the various hydrogen isotopes in the highly convective stellar environment. Therefore, in a helium rich bubble, a fair fraction of the ^{11}B may be converted to ^{14}N, also generating free neutrons, while in hydrogen rich zones this branch remains negligible. A more detailed analysis of the impact of the ^{11}B$(\alpha,n)^{14}$N reaction branch requires complex 3D-simulations, which are beyond the scope of this work.

VI. CONCLUSIONS

This paper presents a new study of the two lowest energy resonances in ^{11}B$(\alpha,n)^{14}$N. The resonance at $E_\alpha =$ 337 keV was measured for the first time by taking advantage of the low cosmogenic neutron background at the CASPAR underground laboratory. The $E_\alpha = 411$ keV resonance was measured for the second time after Wang *et al.* [1] and a consistent value was found for the resonance strength. These two resonances dominate the reaction rate at lower temperatures, such as those found in stellar or also in fusion plasma environments. Previous calculations of the reaction rate used an estimated value for the $E_\alpha = 337$ keV resonance strength. The result from this work is lower than the previously estimated value by two orders of magnitude. This reduction in resonance strength leads to a large reduction in the reaction rate at temperatures below 0.3 GK. At these temperatures the ^{11}B$(\alpha,n)^{14}$N channel was previously considered to be the dominant reaction branch. The new reaction rate results still show the channel to be the dominant reaction branch, but significantly reduce the role of ^{11}B as a contaminating neutron source in stellar and boron

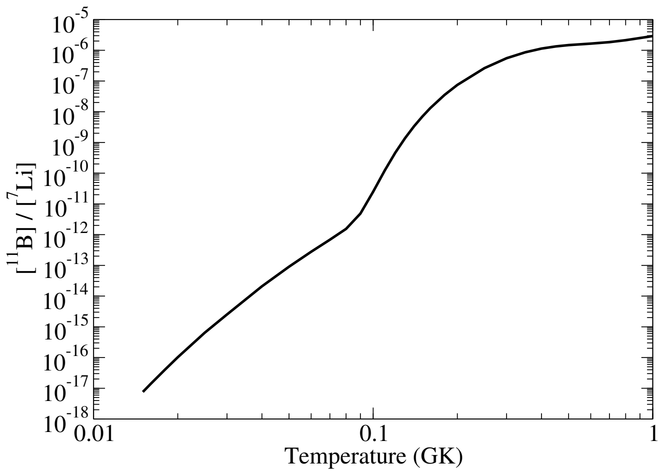

FIG. 9: Ratio of ^{11}B to ^{7}Li in an environment with equal amounts of H and He as a function of temperature as approximated by Eq. (2). Large fluctuation in H, He abundances in the highly convective early star burning environment can lead to drastic deviations from this curve.

plasma environments.

ACKNOWLEDGMENTS

Financial support for this research was provided in part by NSF grant PHY1615197. This research utilized resources from the Notre Dame Center for Research Computing and the research of those from the University of Notre Dame were funded by the National Science Foundation through Grant No. PHY-2011890 (University of Notre Dame Nuclear Science Laboratory) and Grant No. PHY-1430152 (the Joint Institute for Nuclear Astrophysics - Center for the Evolution of the Elements).

[1] T. R. Wang, R. B. Vogelaar, and R. W. Kavanagh, ^{11}B+α reaction rates and primordial nucleosynthesis, Phys. Rev. C **43**, 883 (1991).

[2] J. H. Applegate, Neutron diffusion, primordial nucleosynthesis, and the r-process, Physics Reports **163**, 141 (1988).

[3] R. Malaney and W. Fowler, Origin and Distribution of the Elements (World Scientific, Singapore, 1988) p. 76.

[4] T. Rauscher, J. H. Applegate, J. J. Cowan, F.-K. Thielemann, and M. Wiescher, Production of Heavy Elements in Inhomogeneous Cosmologies, ApJ **429**, 499 (1994).

[5] S. C. Keller, M. S. Bessell, A. Frebel, A. R. Casey, M. Asplund, H. R. Jacobson, K. Lind, J. E. Norris, D. Yong, A. Heger, Z. Magic, G. S. da Costa, B. P. Schmidt, and P. Tisserand, A single low-energy, iron-poor supernova as the source of metals in the star SMSS J031300.36-670839.3, Nature **506**, 463 (2014), arXiv:1402.1517 [astro-ph.SR].

[6] M. S. Bessell, R. Collet, S. C. Keller, A. Frebel, A. Heger, A. R. Casey, T. Masseron, M. Asplund, H. R. Jacobson, K. Lind, A. F. Marino, J. E. Norris, D. Yong, G. Da Costa, C. Chan, Z. Magic, B. Schmidt, and P. Tisserand, Nucleosynthesis in a Primordial Supernova: Carbon and Oxygen Abundances in SMSS J031300.36-670839.3, ApJ **806**, L16 (2015), arXiv:1505.03756 [astro-ph.SR].

[7] A. Arcones and F.-K. Thielemann, Origin of the elements, The Astronomy and Astrophysics Review **31**, 1 (2022).

[8] M. Wiescher, O. Clarkson, R. J. deBoer, and P. Denisenkov, Nuclear clusters as the first stepping stones for the chemical evolution of the universe., The European Physical Journal A **57**, 24 (2021).

[9] O. Clarkson and F. Herwig, Convective H-He interactions in massive population III stellar evolution models, Monthly Notices of the Royal Astronomical Society **500**, 2685 (2020), https://academic.oup.com/mnras/article-pdf/500/2/2685/34546031/staa3328.pdf.

[10] J. A. Liendo, N. R. Fletcher, D. D. Caussyn, K. W. Kemper, and E. E. Towers, ^{15}N cluster states in triton transfer and their alpha decay, Phys. Rev. C **50**, 3155 (1994).

[11] R. E. Azuma, E. Uberseder, E. C. Simpson, C. R. Brune, H. Costantini, R. J. de Boer, J. Görres, M. Heil, P. J. LeBlanc, C. Ugalde, and M. Wiescher, AZURE: An *R*-matrix code for nuclear astrophysics, Phys. Rev. C **81**, 045805 (2010).

[12] R. J. deBoer, J. Görres, M. Wiescher, R. E. Azuma, A. Best, C. R. Brune, C. E. Fields, S. Jones, M. Pignatari, D. Sayre, K. Smith, F. X. Timmes, and E. Uberseder, The $^{12}\mathbf{C}(\alpha,\gamma)^{16}\mathbf{O}$ reaction and its implications for stellar helium burning, Rev. Mod. Phys. **89**, 035007 (2017).

[13] S. Atzeni and J. Meyer-ter Vehn, *The Physics of Inertial Fusion: Beam Plasma Interaction, Hydrodynamics, Hot Dense Matter*, International Series of Monographs on Physics (OUP Oxford, 2004).

[14] F. Consoli, R. De Angelis, P. Andreoli, A. Bonasera, M. Cipriani, G. Cristofari, G. Di Giorgio, D. Giulietti, and M. Salvadori, Diagnostic methodologies of laser-initiated $^{11}\mathrm{B}(\mathrm{p},\alpha)2\alpha$ fusion reactions, Frontiers in Physics **8**, 10.3389/fphy.2020.561492 (2020).

[15] De Angelis, Riccardo, Giulietti, Danilo, Calcagnile, Lucio, Quarta, Gianluca, Andreoli, Pierluigi, Cipriani, Mattia, Consoli, Fabrizio, Cristofari, G., Delle Side, Domenico, Di Giorgio, Giorgio, Ingenito, Francesco, and Maruccio, Lucio, ticle space distribution from fusion reactions in boron irradiated by mono-energetic protons, EPJ Web of Conferences **167**, 05005 (2018).

[16] R. J. deBoer, Q. Liu, Y. Chen, M. Couder, J. Görres, E. Lamere, A. Long, S. Lyons, K. Manukyan, L. Morales, D. Robertson, C. Seymour, G. Seymour, E. Stech, B. V.

Kolk, and M. Wiescher, Global R-matrix analysis of the ^{11}B$(\alpha,n)^{14}$N reaction, Journal of Physics: Conference Series **1668**, 012011 (2020).

[17] D. Robertson, M. Couder, U. Greife, F. Strieder, and M. Wiescher, Underground nuclear astrophysics studies with caspar, Eur. J. Phys. Web of Conferences **109**, 09002 (2016).

[18] A. Gula, R. deBoer, K. Manukyan, and M. Wiescher, The Resonance Structure of the ^{11}B(α,p) Reaction near the α Threshold, unpublished.

[19] S. Falahat, A. Best, M. Couder, J. Görres, K. Kratz, U. Ott, E. Stech, and M. Wiescher, A ^{3}He neutron detector for the measurement of (α,n) reactions, Nucl. Instrum. Meth. A **700**, 53 (2013).

[20] T. C. Borgwardt, *Deep Underground Study of* $^{11}B(\alpha,n)^{14}N$ *and* $^{22}Ne(\alpha,n)^{25}Mg$ *at Low Energies*, Doctoral dissertation, South Dakota School of Mines and Technology (2020).

[21] P. M. Thornewell, *Neutral Current Detectors for the Sudbury Neutrino Observatory*, Doctoral dissertation, University of Oxford (1997).

[22] T. Langford, C. Bass, E. Beise, H. Breuer, D. Erwin, C. Heimbach, and J. Nico, Event identification in ^{3}He proportional counters using risetime discrimination, Nucl. Instrum. Meth. A **717**, 51 (2013).

[23] B. V. Kolk, K. T. Macon, R. J. deBoer, T. Anderson, A. Boeltzig, K. Brandenburg, C. R. Brune, Y. Chen, A. M. Clark, T. Danley, B. Frentz, R. Giri, J. Görres, M. Hall, S. L. Henderson, E. Holmbeck, K. B. Howard, D. Jacobs, J. Lai, Q. Liu, J. Long, K. Manukyan, T. Massey, M. Moran, L. Morales, D. Odell, P. O'Malley, S. N. Paneru, A. Richard, D. Schneider, M. Skulski, N. Sensharma, C. Seymour, G. Seymour, D. Soltesz, S. Strauss, A. Voinov, L. Wüstrich, and M. Wiescher, Investigation of the ^{10}B$(p,\alpha)^{7}$Be reaction from 0.8 to 2.0 MeV, Phys. Rev. C **105**, 055802 (2022).

[24] Q. Liu, M. Febbraro, R. J. deBoer, S. Aguilar, A. Boeltzig, Y. Chen, M. Couder, J. Görres, E. Lamere, S. Lyons, K. T. Macon, K. Manukyan, L. Morales, S. Pain, W. A. Peters, C. Seymour, G. Seymour, R. Toomey, B. V. Kolk, J. Weaver, and M. Wiescher, Low-energy cross-section measurement of the ^{10}B$(\alpha,n)^{13}$N reaction and its impact on neutron production in first-generation stars, Phys. Rev. C **101**, 025808 (2020).

[25] W. A. Fowler, C. C. Lauritsen, and T. Lauritsen, Gamma-radiation from excited states of light nuclei, Rev. Mod. Phys. **20**, 236 (1948).

[26] C. R. Brune and D. B. Sayre, Energy deconvolution of cross-section measurements with an application to the ^{12}C$(\alpha,\gamma)^{16}$O reaction, Nuclear Instruments and Methods in Physics Research Section A: Accelerators, Spectrometers, Detectors and Associated Equipment **698**, 49 (2013).

[27] J. J. Ramirez, R. A. Blue, and H. R. Weller, Multilevel Multichannel Study of the Structure of ^{15}N from 12- to 14-MeV Excitation Energy, Phys. Rev. C **5**, 17 (1972).

[28] M. Niecke, M. Niemeier, R. Weigel, and H. Wirzba-Lorenz, Angular distributions of neutron polarization from the ^{14}C(p, n)^{14}N and ^{11}B(α, n)^{14}N reactions and R-matrix analysis of ^{15}N in the excitation-energy range between 11.5 and 12.5 mev, Nuclear Physics A **289**, 408 (1977).

[29] G. M. Hale, P. G. Young, M. Chadwick, and Z.-P. Chen, New Evaluations of Neutron Cross Sections for ^{14}N and ^{16}O, in *Nuclear Data for Science and Technology*, edited by S. M. Qaim (Springer Berlin Heidelberg, Berlin, Heidelberg, 1992) pp. 921–923.

[30] E. T. Jurney, J. W. Starner, J. E. Lynn, and S. Raman, Thermal-neutron capture by ^{14}N, Phys. Rev. C **56**, 118 (1997).

[31] R. E. Azuma, E. Uberseder, E. C. Simpson, C. R. Brune, H. Costantini, R. J. de Boer, J. Görres, M. Heil, P. J. LeBlanc, C. Ugalde, and M. Wiescher, AZURE: An R-matrix code for nuclear astrophysics, Phys. Rev. C **81**, 045805 (2010).

[32] E. Uberseder and R. J. deBoer, *AZURE2 User Manual* (2015).

[33] C. R. Brune, Alternative parametrization of R-matrix theory, Phys. Rev. C **66**, 044611 (2002).

[34] W. Huang, M. Wang, F. Kondev, G. Audi, and S. Naimi, The AME 2020 atomic mass evaluation (I). Evaluation of input data, and adjustment procedures, Chinese Physics C **45**, 030002 (2021).

[35] M. Wang, W. Huang, F. Kondev, G. Audi, and S. Naimi, The AME 2020 atomic mass evaluation (II). Tables, graphs and references, Chinese Physics C **45**, 030003 (2021).

[36] W. R. Harris and J. C. Armstrong, Elastic Scattering of 1- to 2.7-MeV Protons by C^{14}, Phys. Rev. **171**, 1230 (1968).

[37] J. D. Henderson, E. L. Hudspeth, and W. R. Smith, Capture and Elastic Scattering of Protons by ^{14}C, Phys. Rev. **172**, 1058 (1968).

[38] R. M. Sanders, Study of the C$^{14}(p,n)$N^{14} and C$^{14}(\alpha,n)$O^{17} Reactions, Phys. Rev. **104**, 1434 (1956).

[39] G. Bartholomew, F. Brown, H. Gove, A. Litherland, and E. Paul, Capture Radiation and Neutrons from the Bombardment of C^{14} with Protons, Canadian Journal of Physics **33**, 10.1139/p55-053 (1955).

[40] C. H. Johnson, B. Petree, and R. K. Adair, Total Cross Section of Nitrogen for Fast Neutrons, Phys. Rev. **84**, 775 (1951).

[41] J. J. Hinchey, P. H. Stelson, and W. M. Preston, The Total Neutron Cross Section of Nitrogen, Phys. Rev. **86**, 483 (1952).

[42] J. A. Harvey, N. W. Hill, N. M. Larson, and D. C. Larson, Measurement of the Nitrogen Total Cross Section from 0.5 eV to 50 MeV, and Analysis of the 433-keV Resonance, in *Nuclear Data for Science and Technology*, edited by S. M. Qaim (Springer Berlin Heidelberg, Berlin, Heidelberg, 1992) pp. 729–731.

[43] F. Gabbard, H. Bichsel, and T. Bonner, The disintegration of nitrogen by fast neutrons, Nuclear Physics **14**, 277 (1959).

[44] G. L. Morgan, Cross Sections for the ^{14}N(n,p_0), (n,α_0), and (n,α_1) Reactions from 0.5 to 15 MeV, Nuclear Science and Engineering **70**, 163 (1979).

[45] Khryachkov, V.A., Bondarenko, I.P., Kuzminov, B.D., Semenova, N.N., Sergachev, A.I., Ivanova, T.A., and Giorginis, G., (n,α) reactions cross section research at IPPE, EPJ Web of Conferences **21**, 03005 (2012).

[46] C. H. Johnson and H. H. Barschall, Interaction of Fast Neutrons with Nitrogen, Phys. Rev. **80**, 818 (1950).

[47] H. Leeb, R. J. deBoer, I. Thompson, and P. Dimitriou, *International Nuclear Data Evaluation Network (INDEN) on the Evaluation of Light Elements (3)*, Tech.

Rep. INDC(NDS)-0827 (International Atomic Energy Agency, Vienna, Austria, 2021).

[48] G. Morgan, Cross Sections for the ^{14}N(n, p_0), (n, α_0), and the (n, α_1) reactions from 0.5 to 15 MeV, Nuclear Science and Engineering **70**, 163 (1979).

[49] D. Odell, C. R. Brune, D. R. Phillips, R. J. deBoer, and S. N. Paneru, Performing Bayesian Analyses With `AZURE2` Using `BRICK`: An Application to the ^{7}Be System, Frontiers in Physics **10**, 888476 (2022).

[50] J. Harvey, N. Hill, N. Larson, D. Larson, C. Beasley, and G. Hale, Measurement of the nitrogen total cross section from 0.5 eV to 50 MeV and the analysis of the 433-keV resonance, in *Conf. on Nucl. Data for Sci. and Technol., Juelich Germany* (1991).

[51] G. R. Caughlan and W. A. Fowler, Thermonuclear reaction rates v, Atomic Data and Nuclear Data Tables **40**, 283 (1988).

[52] W. Kohler, H. Schmidt-Böcking, and K. Bethge, Investigation of ^{15}N by the reactions ^{11}B$(^{7}\mathrm{Li}, t)^{15}$N and ^{10}B$(^{7}\mathrm{Li}, d)^{15}$N, Nuclear Physics A **262**, 113 (1976).

[53] G. A. Norton, K. W. Kemper, G. E. Moore, R. J. Puigh, and M. E. Williams-Norton, States in ^{15}N populated by the ^{11}B$(^{6}\mathrm{Li}, d)$ and ^{11}B$(^{7}\mathrm{Li}, t)$ reactions, Phys. Rev. C **13**, 1211 (1976).

[54] F. Ajzenberg-Selove, Energy levels of light nuclei $A = 13$-15, Nuclear Physics A **523**, 1 (1991).

[55] P. E. Koehler and H. A. O'Brien, ^{14}N(n,p)^{14}C cross section from 61 meV to 34.6 keV and its astrophysical implications, Phys. Rev. C **39**, 1655 (1989).

[56] See Supplemental Material at [URL will be inserted by publisher] for the tabulated reaction rate.

[57] Y. Xu, K. Takahashi, S. Goriely, M. Arnould, M. Ohta, and H. Utsunomiya, NACRE II: an update of the NACRE compilation of charged-particle-induced thermonuclear reaction rates for nuclei with mass number $A < 16$, Nuclear Physics A **918**, 61 (2013).